PNAS RESEARCH ARTICLE | CELL BIOLOGY OPEN ACCESS

TRF2 rescues telomere attrition and prolongs cell survival in Duchenne muscular dystrophy cardiomyocytes derived from human iPSCs

Asuka Eguchi[a,b,c], Adriana Fernanda G. S. Gonzalez[a], Sofía I. Torres-Bigio[a,c], Kassie Koleckar[a], Foster Birnbaum[a], Joe Z. Zhang[b,c,d], Vicky Y. Wang[e], Joseph C. Wu[b,c,d], Steven E. Artandi[f,g], and Helen M. Blau[a,b,c,1]

Contributed by Helen M. Blau; received June 9, 2022; accepted December 29, 2022; reviewed by María A. Blasco and Ronald A. DePinho

Duchenne muscular dystrophy (DMD) is a severe muscle wasting disease caused by the lack of dystrophin. Heart failure, driven by cardiomyocyte death, fibrosis, and the development of dilated cardiomyopathy, is the leading cause of death in DMD patients. Current treatments decrease the mechanical load on the heart but do not address the root cause of dilated cardiomyopathy: cardiomyocyte death. Previously, we showed that telomere shortening is a hallmark of DMD cardiomyocytes. Here, we test whether prevention of telomere attrition is possible in cardiomyocytes differentiated from patient-derived induced pluripotent stem cells (iPSC-CMs) and if preventing telomere shortening impacts cardiomyocyte function. We observe reduced cell size, nuclear size, and sarcomere density in DMD iPSC-CMs compared with healthy isogenic controls. We find that expression of just one telomere-binding protein, telomeric repeat-binding factor 2 (TRF2), a core component of the shelterin complex, prevents telomere attrition and rescues deficiencies in cell size as well as sarcomere density. We employ a bioengineered platform to micropattern cardiomyocytes for calcium imaging and perform Southern blots of telomere restriction fragments, the gold standard for telomere length assessments. Importantly, preservation of telomere lengths in DMD cardiomyocytes improves their viability. These data provide evidence that preventing telomere attrition ameliorates deficits in cell morphology, activation of the DNA damage response, and premature cell death, suggesting that TRF2 is a key player in DMD-associated cardiac failure.

Duchenne muscular dystrophy | telomere | cardiomyocytes | induced pluripotent stem cells

Duchenne muscular dystrophy (DMD) affects one out of 5,000 males and manifests as progressive muscle degeneration (1). DMD is caused by mutations in dystrophin, the largest gene in the genome (2). The gene product, dystrophin, has an essential role in connecting the contractile apparatus to the extracellular matrix (3). Dilated cardiomyopathy is the leading cause of death in DMD patients (4). Currently, patients are prescribed angiotensin-converting enzyme inhibitors, angiotensin II receptor blockers, and mineralocorticoid receptor antagonists that lower blood pressure or beta blockers that slow the heart rate (5). These strategies reduce the mechanical load on the heart but do not address the cardiomyocyte death and fibrosis that drive the progression of dilated cardiomyopathy.

We previously reported an intriguing link between genetic cardiomyopathies and telomere shortening. Telomeres are repetitive DNA elements, comprised of the sequence 5′-TTAGGG-3′. The shelterin complex folds the telomeres into T-loop structures that prevent free DNA ends from being recognized as double-stranded breaks and being repaired through homology-directed repair or nonhomologous end joining (6). While the dystrophin-deficient *mdx* mouse does not manifest the characteristic symptoms of DMD, when crossed with an *mTR* knockout mouse that is missing the RNA component of telomerase (7, 8), mdx^{4cv}/mTR^{G2} mice exhibit hallmark DMD features, including severe muscle degeneration, kyphosis, dilated cardiomyopathy, and shortened lifespan (9–11). We and others have capitalized on human-induced pluripotent stem cells (iPSCs) to model cardiac disease phenotypes in a dish in order to surmount differences between human and mouse cells (12–15). We have shown that in cardiomyocytes differentiated from iPSCs (iPSC-CMs) derived from patients harboring mutations in contractile proteins including dystrophin, titin, and troponin T (12), telomeres shorten in conjunction with manifestation of cardiomyocyte deficits (13). Such shortening does not occur in isogenic control iPSC-CMs in which the mutations are CRISPR-corrected (12, 13).

Here, we investigate whether telomere shortening is not just correlated with cardiomyocyte dysfunction but can be abrogated, ameliorating the pathogenic features of DMD cardiomyocytes. We use three DMD iPSC lines with matching healthy control lines and at least three differentiation experiments per line, a robust dataset. Using isogenic controls,

Significance

Patients with Duchenne muscular dystrophy (DMD) exhibit severe skeletal muscle degeneration and die of respiratory or heart failure due to the lack of dystrophin. Previous genetic studies by our lab demonstrated a correlation between short telomeres and human and mouse DMD-associated heart failure. To gain mechanistic insights into the role of telomeres in DMD cardiomyocytes, we model the disease using three independent lines of human-induced pluripotent stem cells harboring mutations in the dystrophin gene and three healthy control lines of matching genetic backgrounds. We find that upregulation of a single telomere-binding protein, TRF2, prevents telomere shortening, restores cardiomyocyte size and sarcomere density, and improves cell survival, providing evidence that preventing telomere attrition is critical for cardiomyocyte function.

Author contributions: A.E. and H.M.B. designed research; A.E., A.F.G.S.G., and K.K. performed research; F.B., J.Z.Z., V.Y.W., J.C.W., and S.E.A. contributed new reagents/analytic tools; A.E., A.F.G.S.G., S.I.T.-B., and K.K. analyzed data; and A.E. and H.M.B. wrote the paper.

Reviewers: M.A.B., Spanish National Cancer Research Centre; R.A.D., The University of Texas MD Anderson Cancer Center.

The authors declare no competing interest.

[1]To whom correspondence may be addressed. Email: hblau@stanford.edu.

This article contains supporting information online at https://www.pnas.org/lookup/suppl/doi:10.1073/pnas.2209967120/-/DCSupplemental.

Published January 31, 2023.

we ensure we control for genetic background and that the differences we observe between healthy and diseased states can be attributed to the dystrophin deficiency. We capitalize on a bioengineered platform to micropattern iPSC-CMs to a physiological length:width aspect ratio for calcium imaging and measure telomere restriction fragments by Southern blot for rigorous assessment of telomere lengths. We also take advantage of a lentiviral cardiac troponin T (cTnT) reporter system with a zeocin resistance gene to enrich for cardiomyocytes. We show that upon expression of just one of the telomere-binding proteins of the multisubunit shelterin complex, telomeric repeat-binding factor 2 (TRF2), telomere shortening is largely prevented. The upregulation of TRF2, in turn, maintains cardiomyocyte size, increases sarcomere content, partially improves calcium handling, and has a major impact on cell survival. These findings provide fresh mechanistic insights in human cells and direct evidence for protection of telomeres as a causal role in preventing cardiomyocyte dysfunction that leads to heart failure.

Results

DMD iPSC as a Disease Model. We differentiated human-iPSCs to cardiomyocytes to model DMD in culture (Table 1 and Fig. 1*A*). Dystrophin, the protein that is missing in DMD, is encoded by the largest gene in the human genome and encompasses 2.4 megabases (16). As a result, DMD can be caused by a wide variety of mutations that impact the function of the dystrophin protein (17). Two lines, DMD19 and DMD16, were derived from patients with nonsense mutations in the dystrophin gene that result in degradation of the transcript by nonsense-mediated mRNA decay (18, 19). Both lines have been CRISPR-corrected to generate corresponding isogenic controls, DMD19 iso and DMD16 iso, in which the dystrophin mutations are corrected (18, 19). A third line, UC3.4, was derived from a healthy individual, and the isogenic DMD line, UC1015.6, was CRISPR-induced to yield a DMD mutation, c.263delG, which results in deletion of the N terminus of dystrophin that renders the truncated protein dysfunctional (20, 21). Importantly, the lack of the N-terminal actin-binding domain of dystrophin is associated with early-onset dilated cardiomyopathy (22). The use of three DMD iPSC lines with matching isogenic healthy controls ensures that results are controlled for genetic background, and consistent differences observed between healthy and diseased states can be attributed to the dystrophin deficiency.

All six iPSC lines were shown to express classic pluripotency markers, OCT4, SOX2, and TRA-1-60, before differentiation (*SI Appendix*, Fig. S1 *A–C*). We differentiated the iPSCs to cardiomyocytes using established protocols (23), then purified the iPSC-CMs by culturing them in media lacking glucose and supplemented with lactate, a method that starves contaminating fibroblasts (24). On day 30, we observed cTnT immunostaining in the iPSC-CMs (Fig. 1*B*). We also immunostained iPSC-CMs for dystrophin and observed expression along the sarcomeres in the healthy control lines, UC3.4, DMD19 iso, and DMD16 iso (Fig. 1*B*). As expected, the DMD lines, DMD19 and DMD16, did not show dystrophin expression along the sarcomeres as they harbor nonsense mutations (Fig. 1*B*) (19). In contrast, the UC1015.6 line has a mutation that induces the expression of a truncated dystrophin lacking a large portion of the N-terminal domain that binds actin filaments (21). Immunostaining with the MANEX1A antibody that recognizes the N terminus of dystrophin encoded by exon 1 showed a lack of expression in the DMD line, UC1015.6 (Fig. 1*B*) (25), and use of the ab15277 antibody that recognizes the C terminus detected the truncated dystrophin (*SI Appendix*, Fig. S2*A*), consistent with the report that this line expresses a dystrophin variant missing the N-terminal actin-binding domain (21). All lines, healthy and DMD alike, showed nuclear staining with the C-terminal antibody. The ubiquitously expressed Dp71 isoform, expressed in human heart tissue and in iPSC-CMs (19, 26, 27), is the protein form likely recognized as none of the mutations we use here preclude expression of this isoform. Taken together, our characterization of the iPSC-CMs demonstrated expression of cardiac-specific markers and muscle-specific dystrophin deficiency in the diseased cells and validated use of these lines as robust disease models to study the role of telomeres in the etiology of DMD.

DMD iPSC-CMs Exhibit Morphological Deficits. We investigated the morphological deficits that could potentially account for functional shortcomings. Previously, we reported that DMD iPSC-CMs exhibit impaired contractile function on stiff substrates mimicking a fibrotic myocardium as well as poor calcium handling (13). On day 30 of differentiation, we observed that DMD iPSC-CMs were smaller in cell size and had smaller nuclei (Fig. 2 *A–I*). The reduced cell size is consistent with our previous report where we seeded iPSC-CMs on 2,000-μm^2 micropatterns of extracellular matrix with a length:width aspect ratio of 7:1 (13, 28), a regimen that has been shown to promote iPSC-CM maturation (29, 30). As shown here, when cultured in monolayers without any physical constraints, the difference in cell sizes were more pronounced. DMD iPSC-CMs were on average ~58% the size of the healthy iPSC-CMs (Fig. 2 *D–F*). Strikingly, in mdx^{4cv}/mTR^{G2} mice, we also observed reduced cardiomyocyte diameter and smaller nuclei in the hearts of the mouse model that phenocopies the severe symptoms observed in Duchenne patients (10). Morphological changes to the nuclei have also been reported in histological characterization of cardiac tissue from DMD patients with signs of nuclear pyknosis, where the chromatin condenses during cell death (31, 32).

The sarcomere density as measured by cTnT signal over cell area was also reduced in DMD iPSC-CMs compared with isogenic controls (Fig. 2 *J–L*). This decrease in cTnT levels was independent of cell size, indicating that DMD iPSC-CMs are both smaller and have fewer sarcomeres. The reduced sarcomere

Table 1. iPSC lines and mutational status

Category	Name	Mutation Type	Description	Reference
Control	UC3.4	None	Isogenic control of UC1015.6	(20, 21)
DMD	UC1015.6	CRISPR-induced	DMD (c.263delG)	(20, 21)
Control	DMD19 iso	None	Isogenic control of DMD19	(18, 19)
DMD	DMD19	Patient-derived	DMD (c.4918_4919delACinsTG)	(18, 19)
Control	DMD16 iso	None	Isogenic control of DMD16	(18, 19)
DMD	DMD16	Patient-derived	DMD (c.10171C > T)	(18, 19)

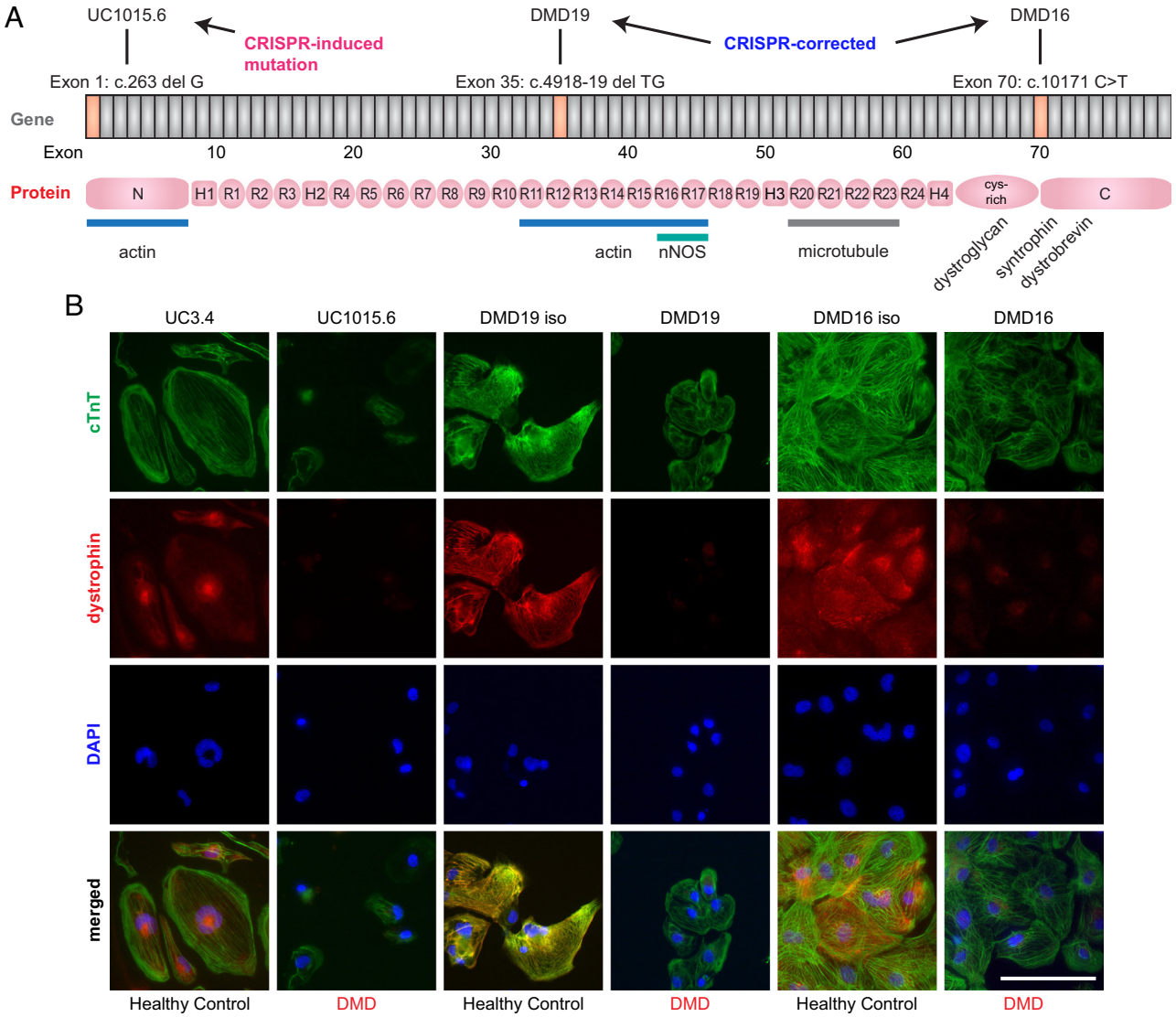

Fig. 1. Cardiomyocytes differentiated from dystrophin-deficient iPSCs. (*A*) Schematic of dystrophin gene and the mutations corresponding to the cell lines. The UC1015.6 line harbors a CRISPR-induced mutation that results in expression of a truncated dystrophin missing the N terminus. DMD19 and DMD16 are patient-derived iPSCs that have nonsense mutations. (*B*) cTnT and dystrophin immunostaining in day 30 iPSC-CMs. The UC lines were stained with the MANEX1A antibody that recognizes the N terminus of dystrophin. The DMD19 and DMD16 lines were stained with the ab15277 antibody that recognizes the C terminus. DAPI in blue marks nuclei. Scale bar, 100 μm.

content likely accounts for the reduced force of contraction, contraction velocity, and relaxation velocity, which we previously measured in these DMD iPSC-CMs (13). Importantly, our findings are consistent with electron micrographs that showed sparse myofibril content in the hearts of DMD patients (31, 32). The reduced cell size, nuclear size, and sarcomere density were statistically significant in all three lines of DMD iPSC-CMs when compared with the healthy isogenic controls, underscoring the consistency of these results. Collectively, the morphological deficits of DMD iPSC-CMs suggest that their smaller cell size as well as reduced sarcomere content impairs their ability to contract like healthy cells.

TRF2 Rescues Telomere Attrition in DMD iPSC-CMs. Previously we determined that telomeres are shortened and that the shelterin complex transcripts are expressed at lower levels in DMD iPSC-CMs (12, 13). We hypothesized that overexpression of a key shelterin protein, TRF2, might suffice to prevent telomere attrition since it is a core protein in the shelterin complex that interacts directly with double-stranded telomeric DNA (Fig. 3*A*) (6, 33). TRF2 directly binds RAP1 and TIN2, mediating recruitment of TPP1 and POT1 (34). In addition, reduced TRF2 levels and telomere shortening have been observed in the hearts of patients with idiopathic and ischemic dilated cardiomyopathy (35). We measured TRF2 levels by western blot and found that DMD iPSC-CMs express lower levels of TRF2 compared with isogenic controls (*SI Appendix*, Fig. S2*B*).

We sought to test whether overexpression of TRF2 on day 10 of differentiation could rescue telomere attrition in DMD iPSC-CMs (Fig. 3*B*). To accurately measure telomere lengths, it was critical to isolate a pure population of iPSC-CMs. In addition to enrichment of the cardiomyocyte population by glucose starvation, we purified the population using a lentiviral reporter system that expresses the zeocin resistance gene (Zeo^R) under the control of the human cTnT promoter (*SI Appendix*, Fig. S2*C*) (36, 37). As a proof-of-concept, we first tested the reporter system that encodes enhanced green fluorescent protein (EGFP) and Zeo^R separated by a T2A self-cleaving peptide (*SI Appendix*, Fig. S2*D*). Colocalization of EGFP with cTnT immunostaining demonstrated that the reporter system provides a reliable method to obtain a pure population of cardiomyocytes (*SI Appendix*, Fig. S2*E*). For

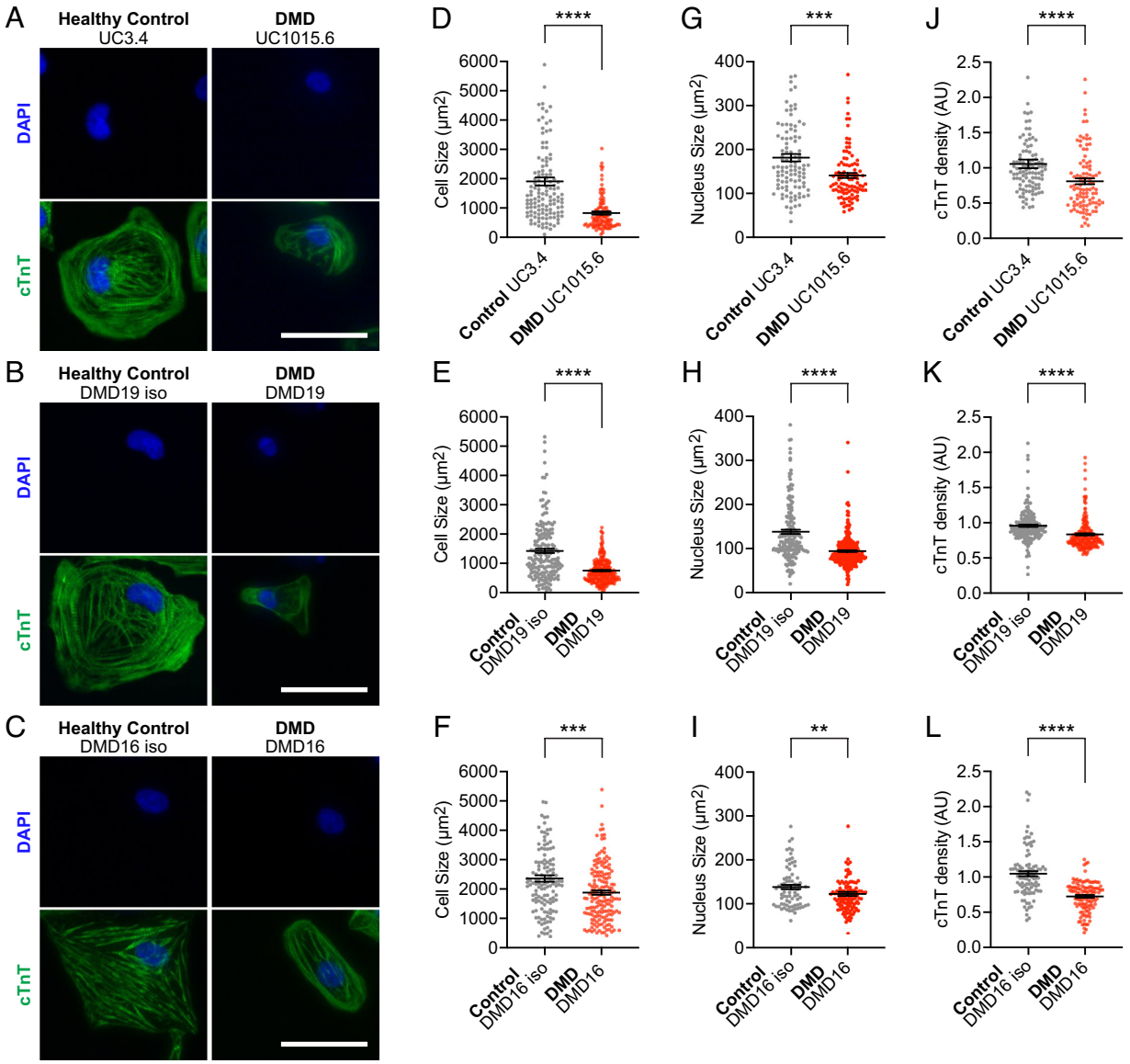

Fig. 2. DMD iPSC-CMs exhibit deficits in cell size, nuclear size, and sarcomere density on day 30 of differentiation. cTnT immunostaining and DAPI staining for nuclei in (*A*) UC3.4 and UC1015.6 iPSC-CMs, (*B*) DMD19 iso and DMD19 iPSC-CMs, and (*C*) DMD16 iso and DMD16 iPSC-CMs. Scale bar, 50 µm. Area of cells for (*D*) UC3.4 and UC1015.6 iPSC-CMs, (*E*) DMD19 iso and DMD19 iPSC-CMs, and (*F*) DMD16 iso and DMD16 iPSC-CMs. Nuclear size for (*G*) UC3.4 and UC1015.6 iPSC-CMs, (*H*) DMD19 iso and DMD19 iPSC-CMs, and (*I*) DMD16 iso and DMD16 iPSC-CMs. Sarcomere density as measured by cTnT signal over cell area for (*J*) UC3.4 and UC1015.6 iPSC-CMs, (*K*) DMD19 iso and DMD19 iPSC-CMs, and (*L*) DMD16 iso and DMD16 iPSC-CMs. Cells were scored from three differentiation experiments. N = 97 to 205 cells. Data shown are mean ± SEM. One-way ANOVA and Mann–Whitney test for post hoc comparison was used to determine significance. **P* < 0.05, ***P* < 0.01, ****P* < 0.001, and *****P* < 0.0001.

subsequent purifications, we used a cTnT reporter that expresses Zeo^R alone that enables purification by zeocin selection. By combining glucose starvation with zeocin selection, we capitalized on two orthogonal purification methods to ensure measurement of telomeres in the cardiomyocyte population.

We measured telomere lengths in purified iPSC-CMs from the six lines by Southern blot of telomere restriction fragments and found that telomeres in DMD cells were shortened (Fig. 3 *C–H*), corroborating our previous findings in DMD iPSC-CMs using quantitative fluorescent in situ hybridization (Q-FISH) (12, 13). Since telomere lengths in pluripotent cells can extend with increased passaging (38, 39), we controlled for passage number before differentiation. Telomere fragment resolution was achieved by running the DNA on low 0.5% agarose gels. We found that TRF2 upregulation significantly prevented telomere attrition in all three lines of DMD iPSC-CMs (Fig. 3 *C–H*). As a negative control for retroviral transduction, we used an empty retroviral vector (ev) with no open reading frame. In comparison with the isogenic controls, the shortest telomeres were significantly shorter in the DMD iPSC-CMs, and these short telomeres were absent following TRF2 upregulation.

As we demonstrated previously by immunofluorescence microscopy, telomere attrition is occurring independently of cell division (13). To sample a greater number of cells compared with our previous report, we measured EdU incorporation in iPSC-CMs by flow cytometry. We used a Live/Dead staining dye, cTnT as a marker for iPSC-CMs, and OCT4 as a marker for iPSCs. We found that 0.5 to 2.8% of iPSC-CMs incorporated EdU between day 20 and day 30 of differentiation compared with 45 to 53% of iPSCs (*SI Appendix*, Fig. S3 *A–H*). Incorporation of EdU contributed to an increase in ploidy without cell division between day 20 and day 30 of differentiation, with 5 to 15% of iPSC-CMs exhibiting a ploidy of 4N or more (*SI Appendix*, Fig. S3 *I* and *J* and Table S1). Measurement of telomerase activity by telomeric

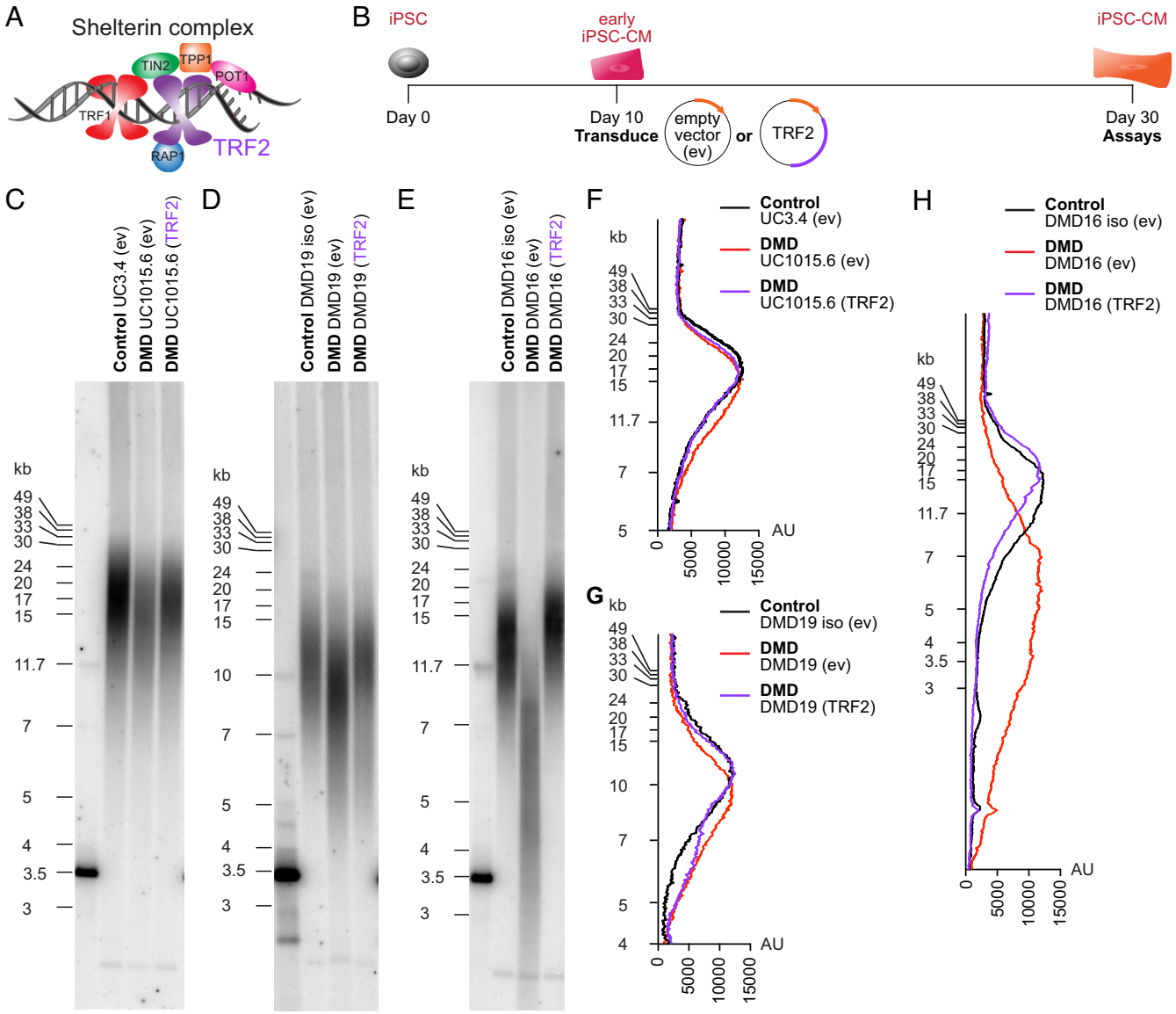

Fig. 3. TRF2 overexpression rescues telomere attrition. (*A*) The shelterin complex is made up of six subunits. TRF1 and TRF2 directly bind telomere sequences. (*B*) On day 10 of differentiation to cardiomyocytes from iPSCs, cells were transduced with an empty retroviral vector with no open reading frame (ev) or TRF2. Assays were performed on day 30 of differentiations. Southern blot of telomere restriction fragments of day 30 iPSC-CMs from (*C*) UC iPSC-CMs, (*D*) DMD19 iPSC-CMs, and (*E*) DMD16 iPSC-CMs. Signal distribution of telomere lengths from the Southern blots in arbitrary units (AU) for (*F*) UC iPSC-CMs, (*G*) DMD19 iPSC-CMs, and (*H*) DMD16 iPSC-CMs.

repeat amplification protocol (TRAP) assay showed no telomerase activity in iPSC-CMs between day 20 and day 30, while robust telomerase activity was measured in the pluripotent controls (*SI Appendix*, Fig. S4 *A–D*).

We previously reported that DMD cardiomyocytes exhibit elevated levels of reactive oxygen species (11, 40). Telomere sequences are rich in guanines, which are susceptible to oxidation to 8-oxoguanine (41). To determine whether oxidized lesions on the telomeres is correlated with telomere attrition, we performed a modified Southern blot of telomere restriction fragments. First, we digested the genomic DNA with MboI and AluI as typically done to enrich for telomeric DNA. Then, we treated with formamidopyrimidine DNA glycosylase (FPG), which removes oxidized nucleobases with 8-oxoguanine being the favored substrate (42). We also treated with S1 nuclease, that degrades single-stranded DNA (*SI Appendix*, Fig. S5*A*). After treatment with only S1 nuclease, we are able to measure the relative abundance of abasic sites with smaller fragments indicating greater frequency of occurrence. After treatment with both FPG and S1 nuclease, we can measure the relative abundance of oxidized lesions (*SI Appendix*, Fig. S5*B*). This modified Southern blot showed that DMD iPSC-CMs exhibited elevated levels of abasic sites and oxidized lesions compared with the healthy isogenic control (*SI Appendix*, Fig. S5*C*). Transduction with TRF2 prevented the accumulation of abasic sites and oxidized lesions (*SI Appendix*, Fig. S5 *D–F*). Collectively, these data show that telomere attrition, a hallmark of cardiac disease progression, occurs independently of cell division, and protection of telomeres with TRF2 curbs this attrition by preventing oxidative damage.

TRF2 Attenuates the DNA Damage Response and Prolongs Cell Survival. While TRF2 protein levels were quite low in the differentiated healthy and DMD iPSC-CMs, when overexpressed, TRF2 levels were significantly elevated in all three lines of DMD iPSC-CMs (Fig. 4*A*). The other subunits of the shelterin complex were not up-regulated upon transduction with TRF2 (*SI Appendix*, Fig. *S6 A–F*). Because TRF2 plays a major role in preserving the

integrity of the telomeres (43, 44), we sought to determine the effects of TRF2 upregulation on the DNA damage response. Specifically, TRF2 inhibits the ataxia-telangiectasia-mutated (ATM)-mediated DNA damage response (43, 44), so we measured levels of p53, which gets up-regulated in response to DNA damage (45), and γ-H2AX, a marker of double-stranded breaks (46). Following TRF2 overexpression, we observed attenuated levels of p53 and γ-H2AX in all three lines of DMD iPSC-CMs (Fig. 4 *B* and *C*). We also measured the levels of phospho-CHK2, the checkpoint effector kinase that is activated in response to double-stranded breaks (47), and total CHK2. We detected low levels of activated CHK2 in all three lines of DMD iPSC-CMs and little to no expression in the healthy control lines and DMD lines treated with TRF2 (Fig. 4*D*). Since less than 2.8% of iPSC-CMs are undergoing DNA replication, the low levels of phospho-CHK2 are in line with the small fraction of cells undergoing checkpoint surveillance. Complementary to our findings, overexpression of a dominant negative mutant of TRF2 or knocking down TRF2 with an antisense oligonucleotide resulted in CHK2 activation and telomere shortening in cardiomyocytes isolated from rats (35). In addition, we compared the survival of DMD iPSC-CMs with and without TRF2 overexpression. We found that TRF2 increased the percentage of cells that survived to day 40 of differentiation from day 30 (Fig. 4 *E*–*G*). This prolongation of cell survival addresses the root cause of dilated cardiomyopathy: the loss of cardiomyocytes that subsequently leads to fibrosis and stiffening of the DMD heart. Collectively, these results show that protection of telomeres with TRF2 attenuates the DNA damage response and prevents the premature loss of cardiomyocytes, potentially delaying fibrosis and tissue stiffening in the DMD heart. This therapeutic strategy may also be relevant to other cardiomyopathies beyond those caused by dystrophin deficiency where telomere attrition is a hallmark of disease progression.

TRF2 Rescues Deficits in Cell Morphology and Improves Calcium Handling. We found that DMD iPSC-CMs exhibited decreased cell size, nuclear size, and sarcomere density compared with their healthy counterparts (Fig. 2 *A*–*L*) and sought to determine if TRF2 upregulation could ameliorate these deficits. We discovered that TRF2 upregulation improved the diminished cell and nuclear size in all three DMD lines (Fig. 5 *A*–*I*). TRF2 upregulation also significantly increased the density of cTnT in UC1015.6 and DMD19 iPSC-CMs (Fig. 5 *J*–*L*).

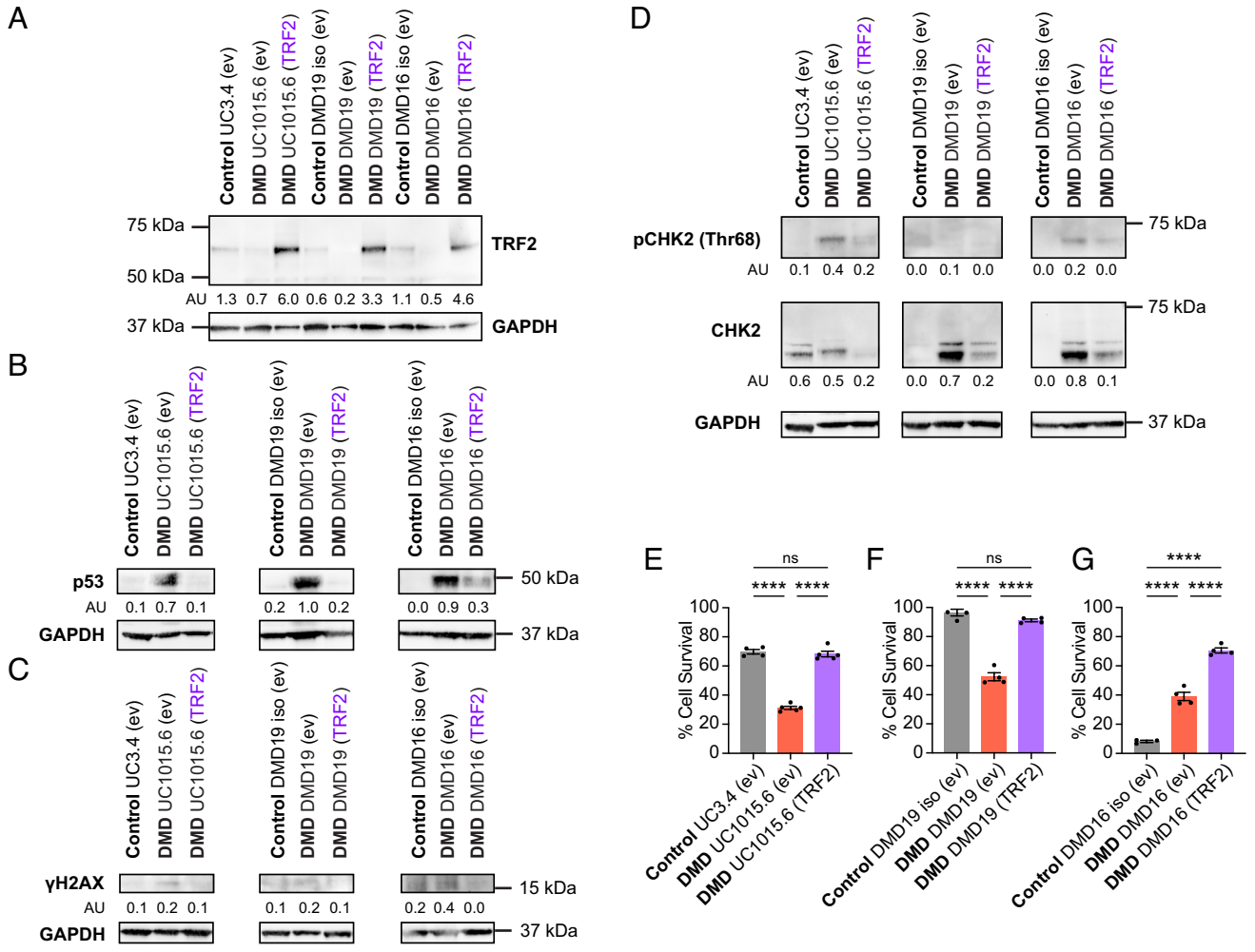

Fig. 4. TRF2 attenuates ATM-mediated DNA damage response and prolongs cell survival. Cells were transduced with ev or TRF2 on day 10 and assayed on day 30. (*A*) Western blot of TRF2 levels with glyceraldehyde-3-phosphate dehydrogenase (GAPDH) as a loading control. TRF2 signal normalized to GAPDH signal in AU. The expected sizes are 65 kDa for TRF2 and 35 kDa for GAPDH. (*B*) Western blot of P53 normalized to GAPDH signal in AU. The expected size for P53 is 50 kDa. (*C*) Western blot of gH2AX normalized to GAPDH signal in AU. The expected size for gH2AX is 17 kDa. (*D*) Western blot of CHK2 phosphorylated at threonine 68 and total CHK2. Signals are normalized to GAPDH signal in AU. The expected size of phosphor-CHK2 is 62 kDa. Percentage of cells that survived on day 40 when compared with day 30 of differentiation for (*E*) UC iPSC-CMs, (*F*) DMD19 iPSC-CMs, and (*G*) DMD16 iPSC-CMs. Survival was scored from three to five differentiation experiments. N = 375 to 12,036 cells on day 30. Data shown are mean ± SEM. One-way ANOVA and Tukey test for post hoc comparison were used to calculate significance. ****$P < 0.0001$.

In DMD cardiomyocytes, dystrophin deficiency leads to a leaky plasma membrane that causes elevated calcium levels and poor calcium handling, which correlates with arrhythmia. To evaluate the effect of TRF2 on cardiomyocyte function, we performed calcium imaging using the ratiometric calcium dye, Fura Red AM. We micropatterned iPSC-CMs at a 7:1 length:width aspect ratio on glass-bottomed wells (*SI Appendix*, Fig. S7*A*), a bioengineering method that we and others showed promotes parallel alignment of the myofibrils and improves the maturity of iPSC-CMs (13, 28, 29). TRF2 transduction restored the transient amplitude for UC1015.6 iPSC-CMs to levels comparable to the healthy isogenic control, UC3.4 iPSC-CMs, under conditions of pacing at 1 Hz, an electrical stimulation that induces contraction at one-second intervals (*SI Appendix*, Fig. S7 *B* and *C*). While other parameters of calcium handling, including time to peak, peak duration, and peak frequency, showed a partial rescue, none improved to statistically significant levels (*SI Appendix*, Fig. S7 *D–N*).

We characterized the types of traces for each cell as class I (traces with regular peaks at 1-s intervals), class II (traces that deviate slightly from the 1-s intervals and show signs of early afterdepolarization), and class III (traces that deviate significantly from the 1-s intervals) (*SI Appendix*, Fig. S8*A*). Early afterdepolarization

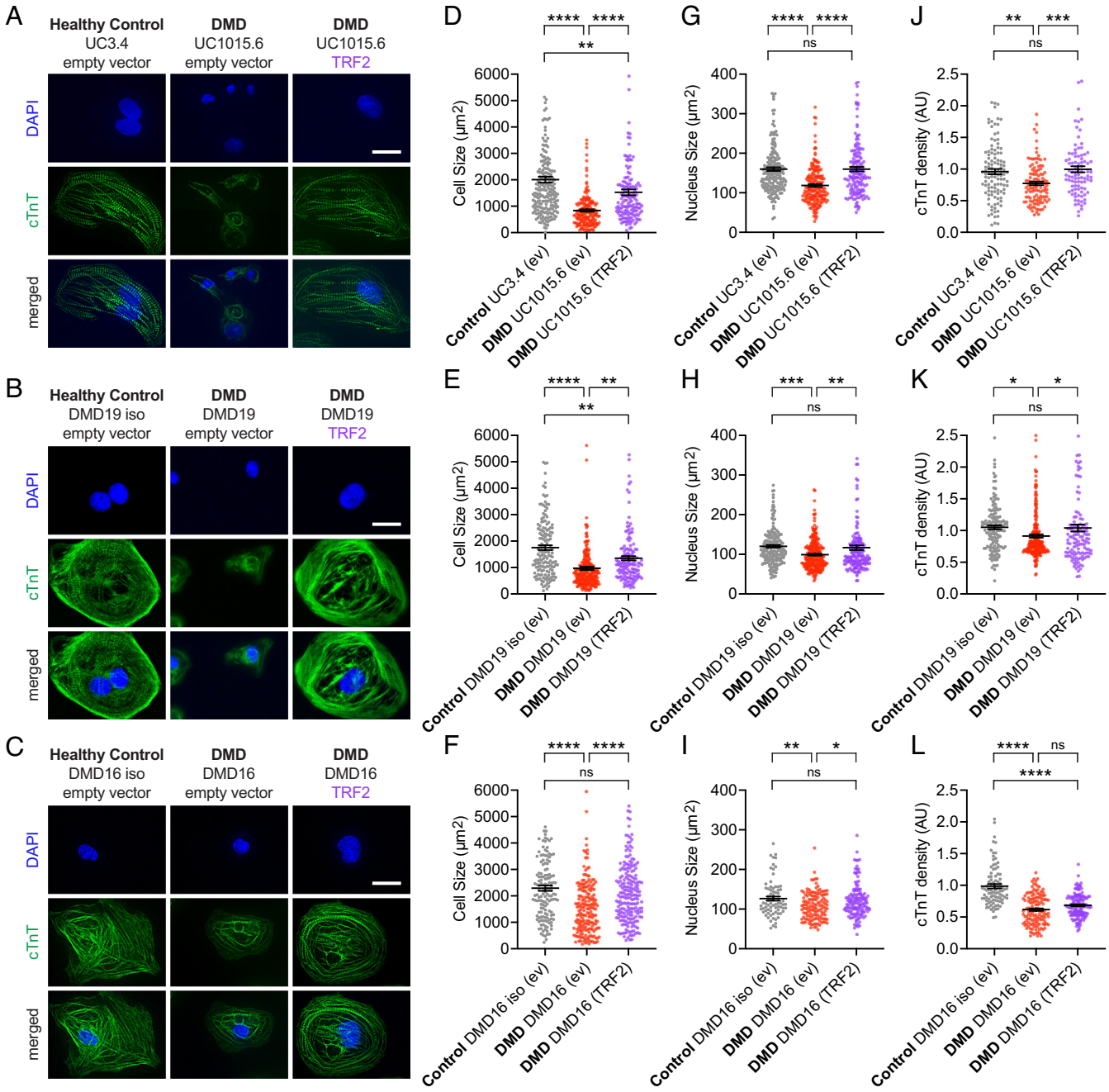

Fig. 5. TRF2 rescues deficits in cell size, nuclear size, and sarcomere density. Cells were transduced with ev or TRF2 on day 10 and assayed on day 30. cTnT immunostaining and DAPI staining for nuclei in (*A*) UC iPSC-CMs, (*B*) DMD19 iPSC-CMs, and (*C*) DMD16 iPSC-CMs. Scale bar, 20 μm. Area of cells for (*D*) UC iPSC-CMs, (*E*) DMD19 iPSC-CMs, and (*F*) DMD16 iPSC-CMs. Nuclear size for (*G*) UC iPSC-CMs, (*H*) DMD19 iPSC-CMs, and (*I*) DMD16 iPSC-CMs. Sarcomere density as measured by cTnT signal over cell area for (*J*) UC iPSC-CMs, (*K*) DMD19 iPSC-CMs, and (*L*) DMD16 iPSC-CMs. Cells were scored from three differentiation experiments. N = 90 to 230 cells. Data shown are mean ± SEM. One-way ANOVA and Tukey test for post hoc comparison were used to determine significance. **P* < 0.05, ***P* < 0.01, ****P* < 0.001, and *****P* < 0.0001.

events show calcium spikes within the decay phase of the calcium transients and can cause lethal arrhythmias (48); therefore, correction of such events would have a meaningful impact on preventing heart failure. As the iPSC-CMs are paced at 1 Hz, calcium transients should oscillate at regular 1-s intervals. Indeed, for the healthy control iPSC-CMs, the majority of cells exhibited class I traces (*SI Appendix*, Fig. S8 *B–D* and Table S2). For the UC and DMD19 lines, DMD iPSC-CMs showed significantly higher frequencies of aberrant calcium handling of class II and III trace types (*SI Appendix*, Fig. S8 *B* and *C*).

For each cell imaged, we calculated an arrhythmia score based on variance in amplitude, frequency, and variance in transient duration (*SI Appendix*, Fig. S8*E*). The scoring system was established on a nine-point scale with one point derived from amplitude variance and nine points on frequency and transient duration variance. As the iPSC-CMs are paced at 1 Hz, calcium transients should oscillate at regular 1-s intervals and show low arrhythmia scores. High arrhythmia scores were indicative of high frequency of calcium oscillations and aberrant calcium handling. Indeed, for the healthy control iPSC-CMs, the majority of cells exhibited low arrhythmia scores (*SI Appendix*, Fig. S8 *F–H*). By contrast, the majority of cells from the DMD lines, UC1015.6 and DMD19, showed high arrhythmia scores (*SI Appendix*, Fig. S8 *F* and *G*). Transduction with TRF2 in DMD iPSC-CMs reduced the number of cells with high arrhythmia scores; however, reduction was not statistically significant (*SI Appendix*, Fig. S8 *F–H*). These results collectively demonstrate that TRF2 upregulation not only confers telomere protection and prevents telomere attrition but provides morphological advantages that impart some functional improvements to DMD iPSC-CMs but does not fully restore the ability to regulate calcium levels.

Dominant-Negative TRF2 Does Not Lead to Telomere Attrition. To determine whether deprotection of telomeres is sufficient to induce telomere attrition, we overexpressed TRF2$^{\Delta B\Delta M}$ in healthy control iPSC-CMs. TRF2$^{\Delta B\Delta M}$ lacks the N-terminal basic domain and the C-terminal Myb DNA-binding domain (49). This dominant-negative form of TRF2 strips endogenous TRF2 from the telomeres (49). Overexpression of TRF2$^{\Delta B\Delta M}$ did not lead to telomere shortening (*SI Appendix*, Fig. S9 *A* and *B*). Cell size was also not affected; however, nuclear size and sarcomere density were compromised with overexpression of TRF2$^{\Delta B\Delta M}$. (*SI Appendix*, Fig. S9 *C–F*). These data suggest that deprotection alone is not sufficient to induce telomere attrition; additional insults in DMD cardiomyocytes, such as oxidative stress, are necessary to induce telomere dysfunction and subsequent cell death. We propose a model in which reactive oxygen species in DMD iPSC-CMs leads to oxidized nucleobases, namely 8-oxoguanine, that results in accumulation of abasic sites (Fig. 6). These lesions in the telomeres are not repaired, resulting in a persistent activation of the ATM-mediated DNA damaged response. The buildup of abasic sites can eventually lead to telomere attrition, triggering cell death. The overexpression of TRF2 prevents the accumulation of oxidized lesions, thereby promoting cell survival.

Discussion

This study provides evidence that protection of telomeres plays a causal role in preventing the pathological features of DMD. We show that increased expression of TRF2, one of the six subunits in the shelterin complex, suffices to curb telomere attrition, which in turn, restores morphological deficits observed in DMD iPSC-CMs, subdues the DNA damage response, and prolongs cells survival. Our previous study on histological sections of human heart tissue exhibited telomeres that were shorter in DMD patient cardiomyocytes compared with age-matched healthy controls (12), underscoring the correlation between telomere attrition and dilated cardiomyopathy.

To gain insights into the role of telomere shortening in the demise of DMD cardiomyocytes, we used human iPSCs as a disease model (13). Here, we validate telomere attrition by Southern blotting of telomere restriction fragments, the gold standard for telomere length measurements, which reinforces our previous

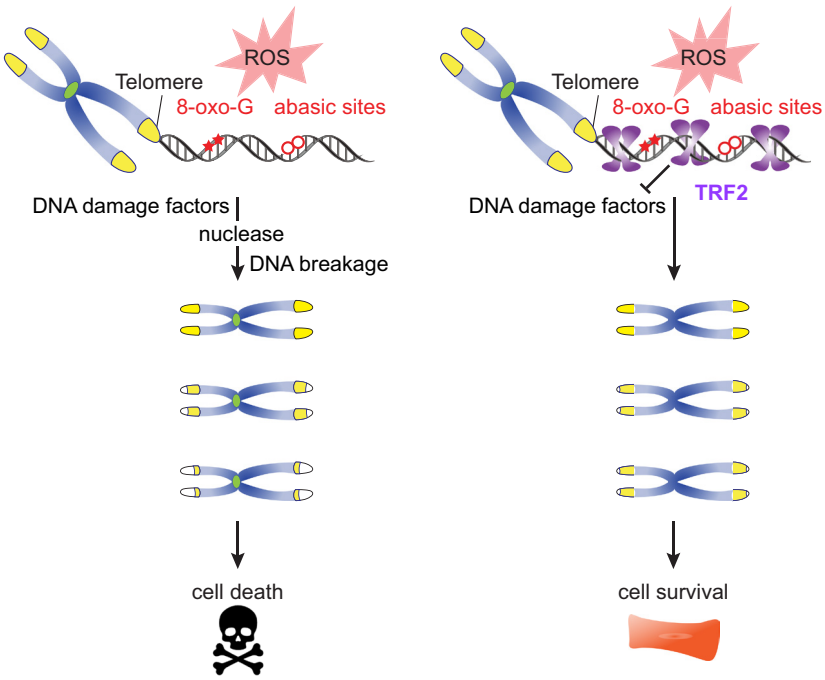

Fig. 6. Model for protection of telomeres by TRF2. Due to the absence of dystrophin, reactive oxygen species in DMD iPSC-CMs lead to 8-oxoguanine lesions and abasic sites. Uncapped telomeres become subject to attrition through DNA damage and activity of nucleases, triggering cell death. Upregulation of TRF2 occludes the binding of DNA damage factors and promotes cell survival.

finding obtained by Q-FISH and monochrome multiplex quantitative PCR (12, 13). Telomere shortening occurs in the absence of cell division, suggesting direct damage to the telomeres as the culprit of attrition. The strength of our findings is underscored by the use of three DMD lines and three isogenic controls where the dystrophin mutations are corrected. Importantly, we demonstrate that reduced cell size, decreased sarcomere density, activation of the DNA damage response, and poor viability can be rescued, underscoring the therapeutic potential of telomere protection. While we observed signs of improved calcium handling in the DMD iPSC-CMs, functional rescue was not significantly restored. Since the diseased cardiomyocytes still lack dystrophin expression, these results suggest that calcium transients are dependent on appropriate dystrophin expression. The plasma membrane is likely still compromised in DMD iPSC-CMs, and calcium can leak into the cell, interfering with proper calcium handling.

We hypothesized that telomere attrition plays a role in the cardiac failure seen in DMD patients and sought to rescue pathogenic features observed in vitro in DMD iPSC-CMs by protecting telomeres. Oxidative stress is elevated in DMD cardiomyocytes (50), and in *mdx* cardiomyocytes, mechanical contraction leads to NOX2-mediated release of reactive oxygen species (51). Direct oxidative damage to the telomeres may lead to persistent activation of the DNA damage response (52), which would be detrimental to cardiomyocytes (53). TRF2, a core subunit of the shelterin complex, can repress the ATM-mediated DNA damage response (43, 44), inhibit binding of poly (ADP-ribose) polymerase 1 (PARP1) to telomeres (54), and prevent hyperresection of telomeres by exonucleases (55). Notably, the rescue of telomere attrition and enhanced cell survival were observed regardless of mutation underscoring the critical role of telomeres in the etiology of DMD. While studies by others have demonstrated that TRF2 overexpression in proliferating cells induces telomere shortening and telomere fusions as a result of XPF nuclease and stalling at the replication fork (56, 57), our study demonstrates that TRF2 overexpression prevents telomere attrition in iPSC-CMs that are not undergoing DNA replication. The mechanism of telomere shortening in postmitotic DMD cardiomyocytes and the role of TRF2 in preventing this shortening remain to be explored. Overexpression of dominant-negative TRF2 in healthy iPSC-CMs was not sufficient to induce telomere attrition, emphasizing the relevance of other cellular stressors in DMD iPSC-CMs that leads to telomere dysfunction.

Protection of telomeres by TRF2 can potentially be a therapeutic strategy to ameliorate other cardiovascular diseases where we and others have observed telomere attrition (12, 35, 58, 59). Our findings of preventing telomere attrition in DMD fit well with prior pioneering research showing that telomerase gene therapy reverses aplastic anemia and pulmonary fibrosis in mice through telomere elongation (60, 61). Our observations of TRF2 in DMD are also in line with the groundbreaking discovery that another subunit of the shelterin complex, TRF1, prolongs the lifespan of mice and protect against anemia and metabolic dysregulation during aging (62). The attenuation of the DNA damage response may have downstream effects on mitochondrial biogenesis through peroxisome proliferator-activated receptor gamma coactivator-1 alpha (PGC-1α) (8, 63). While TRF2 does not replace the function of dystrophin, TRF2 can delay the premature loss of cardiomyocytes, which sets in motion fibrosis and stiffening of the heart tissue that accelerates the development of dilated cardiomyopathy. Our findings suggest that preserving telomere lengths plays a critical role in maintaining cardiomyocyte function and viability.

Materials and Methods

Statistics. Normality of distribution was determined by the Kolmogorov–Smirnov test. For normally distributed data, the unpaired 2-tailed *t* test was used for two samples. For samples that were not normally distributed, the Mann–Whitney test was used to compare two samples. For data sets with more than two samples, one-way ANOVA followed by a post hoc Tukey test was used to determine significance of normally distributed samples. When data were not normally distributed, the Kruskal–Wallis test was used to compare more than two samples. For categorical data, Pearson's chi-square test followed by a z-test with Bonferroni correction was performed for pairwise comparisons to determine whether the observed frequency distributions were different among conditions.

Differentiation to Cardiomyocytes. For maintenance of iPSCs, cells were seeded on Matrigel (Corning 356231)-coated plates and were cultured in Nutristem media (Reprocell 01-0005) with daily medium change. For differentiation to cardiomyocytes, iPSCs were cultured to 70 to 90% confluency and cultured in RPMI-1640 supplemented with 1X B27 minus insulin and 4 to 6 μM CHIR-99021 (Selleck S2924). Two days later, cells were refreshed with RPMI-1640 supplemented with 1X B27 minus insulin and 5 μM IWR-1 (Sigma-Aldrich I0161). Two days later, cells were refreshed in RPMI-1640 supplemented with 1X B27 minus insulin. Two days later, cells were refreshed in RPMI-1640 supplemented with 1X B27 and maintained for 4 d with a medium change every other day. From day 10 of differentiation onward, iPSC-CMs were maintained in RPMI-1640 minus glucose supplemented with 1X B27 and 4 mM lactate (Sigma-Aldrich L7900) with medium change every other day. On day 10, iPSC-CMs were transduced with TRF2 or an empty control retrovirus with 8 μg/mL polybrene. Media were changed every two days. On day 15, cells were harvested with Accutase:TrypLE (1:1 v/v) and replated on Matrigel-coated plates in RPMI-1640 minus glucose supplemented with 1X B27, 4 mM lactate, 5% KSR, and 10 μM Y-27632. On day 16, iPSC-CMs were transduced with TNNT2-zeo. On days 18 to 19, cardiomyocytes were selected for resistance to zeocin (20 μg/mL). All assays were performed on day 30 of differentiation.

Cloning Viral Vectors. Human TRF2 under control of a CMV promoter was expressed from pLPC-TRF2, a gift from Titia de Lange (Addgene plasmid #18002). A short cassette without an open reading frame flanked by HindIII and EcoRI sites was cloned into pLPC-TRF2 to generate the pLPC-Empty plasmid. TroponinT-GCaMP5-Zeo was a gift from John Gearhart (Addgene plasmid #46027). GCaMP5 was substituted for EGFP to generate TroponinT-EGFP-Zeo using the NheI and AgeI sites. A vector expressing the zeocin resistance gene only, TroponinT-Zeo, was created by cloning the zeocin resistance gene between the NheI and AgeI sites.

Virus Production. Retrovirus was produced in Phoenix Amphotropic cells by transfection with FUGENE 6 (Promega E2692) of pLPC-TRF2 or pLPC-Empty. Lentivirus was produced in HEK293T cells by transfection with FUGENE 6 of TNNT2-Zeo or TNNT2-GFP-Zeo, psPAX2 packaging, and pMD2.G envelope plasmids. Media containing virus were harvested 78 h posttransfection. Retrovirus or lentivirus was concentrated using Lenti-X Concentrator (Takara Bio 631231) using the manufacturer's protocol.

Immunofluorescence. For immunostaining, cells were fixed on glass slides and immunostained with appropriate antibodies. Images were acquired on a Ziess Axio Imager Z1 microscope. See *SI Appendix*, Extended Materials and Methods for details.

Western Blot. Proteins from cell lysates were separated by SDS-PAGE and transferred to a nitrocellulose membrane. The membrane was incubated with appropriate antibodies and imaged by chemiluminescence. See *SI Appendix*, Extended Materials and Methods for details.

Telomere Restriction Fragment Southern Blot. Digested genomic DNA was run on an agarose gel and transferred to a Hybond N membrane. Telomeric DNA was visualized using a P32 end-labeled $GGGTTA_3$ probe. See *SI Appendix*, Extended Materials and Methods for details.

Calcium Imaging. Ratiometric calcium imaging with Fura Red was performed on a Zeiss AxioObserver inverted microscope. See *SI Appendix*, Extended Materials and Methods for details.

Cell Viability Assay. Calcein Blue, AM (Thermo Fisher C34853) was used to measure viability on day 30 and day 40 of differentiation. Cells were incubated with 5 μM Calcein Blue for 15 min at 37 °C. After dye uptake, cells were imaged in RPMI 1640 without phenol red and glucose supplemented with 1X B27 and 4 mM lactate. Images of the same field were captured with a 10× objective on a Keyence microscope. The percentage of cells that survived was calculated by dividing the number of cells fluorescently labeled on day 40 by the number on day 30.

Flow Cytometry. iPSCs were pulsed with 20 μM EdU for 1 h using the Click-iT EdU Alexa Fluor 647 Flow kit (Thermo Fisher C10424). iPSC-CMs were pulsed with 10 μM EdU for 24 h. Cells were stained with LIVE/DEAD Fixable Red Dead Cell Stain (Thermo Fisher L23102) using the manufacturer's protocol before fixing in 4% paraformaldehyde. Click-iT labeling of EdU was performed using the manufacturer's protocol. iPSCs were stained with OCT4 (Millipore MAB4419; 1:100 dilution) and iPSC-CMs were stained with cTnT (Thermo Fisher MA5-12960, 1:200 dilution) for 1 h at room temperature. Cells were incubated with goat-anti-rabbit Alexa 488 (Jackson Immuno Research 111-546-045, 1:250 dilution) for 30 min at room temperature. DNA was stained with FxCycle Violet Flow Reagent (Thermo Fisher R37166) using the manufacturer's protocol. Four-color flow cytometry analysis was performed on the SONY SH800 using unstained samples and fluorescence minus one controls to set detectors. FlowJo v10 was used to analyze flow cytometry data.

Data, Materials, and Software Availability. All study data are included in the article and/or *SI Appendix*.

ACKNOWLEDGMENTS. We are grateful to David L. Mack, Martin K. Childers, and Chris Denning for providing the iPSC lines. We acknowledge Garry P. Nolan for providing the Phoenix Amphotropic cells. This work was supported by the American Heart Association (18POST33960526 to A.E. and 17CSA33590101 to H.M.B.), Stanford School of Medicine Dean's Postdoctoral Fellowship (A.E.), Muscular Dystrophy Association (https://doi.org/10.55762/pc.gr.157032), Stanford Translational Research and Applied Medicine Pilot Grant (A.E.), the Stanford Bio-X Summer Undergraduate Research Program (F.B.), a Major Grant from the Stanford University Vice Provost for Undergraduate Education (F.B.), Stanford Undergraduate URM Summer Cardiovascular Research Program R25HL147666 (S.I.T.-B.), California Institute for Regenerative Medicine Bridges to Stem Cell Research Program EDUC2-08382 (A.F.G.S.G.), Tobacco-Related Disease Research Program Fellowship 26FT-0029 (J.Z.Z.), the NIH R01 HL126527 (J.C.W.), R01 HL130020 (J.C.W.), R01 HL123968 (J.C.W.), R01 HL146690 (J.C.W.), R01 HL159340 (H.M.B.), the Keck Foundation (H.M.B.), the Baxter Foundation (H.M.B.), and the Li Ka Shing Foundation (H.M.B.). For statistical analysis, we consulted the Stanford's Data Studio, supported by the National Center for Advancing Translational Sciences of the NIH under Award Number UL1TR003142.

Author affiliations: [a]Baxter Laboratory for Stem Cell Biology, Department of Microbiology and Immunology, Stanford School of Medicine, Stanford, CA 94305; [b]Institute for Stem Cell Biology and Regenerative Medicine, Stanford University School of Medicine, Stanford, CA 94305; [c]Stanford Cardiovascular Institute, Stanford University School of Medicine, Stanford, CA 94305; [d]Division of Cardiology, Department of Medicine, Stanford University School of Medicine, Stanford, CA 94305; [e]Stanford Department of Radiology, Stanford University School of Medicine, Stanford, CA 94305; [f]Stanford Cancer Institute, Stanford University School of Medicine, Stanford, CA 94305; and [g]Department of Biochemistry, Stanford University School of Medicine, Stanford, CA 94035

1. E. M. McNally *et al.*, Contemporary cardiac issues in Duchenne muscular dystrophy. *Circulation* **131**, 1590–1598 (2015).
2. Q. Q. Gao, E. M. McNally, The dystrophin complex: Structure, function, and implications for therapy. *Compr. Physiol.* **5**, 1223–1239 (2015).
3. T. L. E. van Westering, C. A. Betts, M. J. A. Wood, Current understanding of molecular pathology and treatment of cardiomyopathy in Duchenne muscular dystrophy. *Mol. Basel Switz.* **20**, 8823–8855 (2015).
4. G. Nigro, L. I. Comi, L. Politano, R. J. Bain, The incidence and evolution of cardiomyopathy in Duchenne muscular dystrophy. *Int. J. Cardiol.* **26**, 271–277 (1990).
5. F. Kamdar, D. J. Garry, Dystrophin-deficient cardiomyopathy. *J. Am. Coll. Cardiol.* **67**, 2533–2546 (2016).
6. D. Chakravarti, K. A. LaBella, R. A. DePinho, Telomeres: History, health, and hallmarks of aging. *Cell* **184**, 306–322 (2021).
7. A. Leri *et al.*, Ablation of telomerase and telomere loss leads to cardiac dilatation and heart failure associated with p53 upregulation. *EMBO J.* **22**, 131–139 (2003).
8. E. Sahin *et al.*, Telomere dysfunction induces metabolic and mitochondrial compromise. *Nature* **470**, 359–365 (2011).
9. A. Sacco *et al.*, Short telomeres and stem cell exhaustion model Duchenne muscular dystrophy in mdx/mTR mice. *Cell* **143**, 1059–1071 (2010).
10. F. Mourkioti *et al.*, Role of telomere dysfunction in cardiac failure in Duchenne muscular dystrophy. *Nat. Cell Biol.* **15**, 895–904 (2013).
11. A. C. Y. Chang *et al.*, Telomere shortening and metabolic compromise underlie dystrophic cardiomyopathy. *Proc. Natl. Acad. Sci. U.S.A.* **113**, 13120–13125 (2016).
12. A. C. Y. Chang *et al.*, Telomere shortening is a hallmark of genetic cardiomyopathies. *Proc. Natl. Acad. Sci. U. S. A.* **115**, 9276–9281 (2018).
13. A. C. Y. Chang *et al.*, Increased tissue stiffness triggers contractile dysfunction and telomere shortening in dystrophic cardiomyocytes. *Stem. Cell Rep.* **16**, 1–13 (2021).
14. H. Wu *et al.*, Modelling diastolic dysfunction in induced pluripotent stem cell-derived cardiomyocytes from hypertrophic cardiomyopathy patients. *Eur. Heart J.* **40**, 3685–3695 (2019).
15. J. Z. Zhang *et al.*, A human iPSC double-reporter system enables purification of cardiac lineage subpopulations with distinct function and drug response profiles. *Cell Stem. Cell* **24**, 802–811.e5 (2019).
16. M. Koenig *et al.*, Complete cloning of the Duchenne muscular dystrophy (DMD) cDNA and preliminary genomic organization of the DMD gene in normal and affected individuals. *Cell* **50**, 509–517 (1987).
17. C. L. Bladen *et al.*, The TREAT-NMD DMD global database: Analysis of more than 7,000 Duchenne muscular dystrophy mutations. *Hum. Mutat.* **36**, 395–402 (2015).
18. E. Dick *et al.*, Two new protocols to enhance the production and isolation of human induced pluripotent stem cell lines. *Stem. Cell Res.* **6**, 158–167 (2011).
19. E. Dick *et al.*, Exon skipping and gene transfer restore dystrophin expression in human induced pluripotent stem cells-cardiomyocytes harboring DMD mutations. *Stem. Cells Dev.* **22**, 2714–2724 (2013).
20. X. Guan *et al.*, Dystrophin-deficient cardiomyocytes derived from human urine: New biologic reagents for drug discovery. *Stem. Cell Res.* **12**, 467–480 (2014).
21. J. M. Pioner *et al.*, Absence of full-length dystrophin impairs normal maturation and contraction of cardiomyocytes derived from human-induced pluripotent stem cells. *Cardiovasc. Res.* **116**, 368–382 (2020).
22. R. W. Kaspar *et al.*, Analysis of dystrophin deletion mutations predicts age of cardiomyopathy onset in Becker muscular dystrophy. *Circ. Cardiovasc. Genet.* **2**, 544–551 (2009).
23. X. Lian *et al.*, Robust cardiomyocyte differentiation from human pluripotent stem cells via temporal modulation of canonical Wnt signaling. *Proc. Natl. Acad. Sci. U.S.A.* **109**, E1848–E1857 (2012).
24. S. Tohyama *et al.*, Distinct metabolic flow enables large-scale purification of mouse and human pluripotent stem cell-derived cardiomyocytes. *Cell Stem Cell* **12**, 127–137 (2013).
25. T. T. Le *et al.*, Monoclonal antibodies against the muscle-specific N-terminus of dystrophin: Characterization of dystrophin in a muscular dystrophy patient with a frameshift deletion of exons 3–7. *Am. J. Hum. Genet.* **53**, 131–139 (1993).
26. R. C. Austin, P. L. Howard, V. N. D'Souza, H. J. Klamut, P. N. Ray, Cloning and characterization of alternatively spliced isoforms of Dp71. *Hum. Mol. Genet.* **4**, 1475–1483 (1995).
27. S. Jelinkova *et al.*, DMD pluripotent stem cell derived cardiac cells recapitulate in vitro human cardiac pathophysiology. *Front. Bioeng. Biotechnol.* **8**, 535 (2020).
28. F. Birnbaum, A. Eguchi, G. Pardon, A. C. Y. Chang, H. M. Blau, Tamoxifen treatment ameliorates contractile dysfunction of Duchenne muscular dystrophy stem cell-derived cardiomyocytes on bioengineered substrates. *NPJ Regen. Med.* **7**, 19 (2022).
29. A. J. S. Ribeiro *et al.*, Contractility of single cardiomyocytes differentiated from pluripotent stem cells depends on physiological shape and substrate stiffness. *Proc. Natl. Acad. Sci. U.S.A.* **112**, 12705–12710 (2015).
30. D. T. Paik, M. Chandy, J. C. Wu, Patient and disease-specific induced pluripotent stem cells for discovery of personalized cardiovascular drugs and therapeutics. *Pharmacol. Rev.* **72**, 320–342 (2020).
31. H. Nomura, K. Hizawa, Histopathological study of the conduction system of the heart in Duchenne progressive muscular dystrophy. *Acta Pathol. Jpn.* **32**, 1027–1033 (1982).
32. S. Wakai *et al.*, Electron microscopic study of the biopsied cardiac muscle in Duchenne muscular dystrophy. *J. Neurol. Sci.* **84**, 167–175 (1988).
33. F. Erdel *et al.*, Telomere recognition and assembly mechanism of mammalian shelterin. *Cell Rep.* **18**, 41–53 (2017).
34. T. de Lange, Shelterin-mediated telomere protection. *Annu. Rev. Genet.* **52**, 1–25 (2018).
35. H. Oh *et al.*, Telomere attrition and Chk2 activation in human heart failure. *Proc. Natl. Acad. Sci. U.S.A.* **100**, 5378–5383 (2003).
36. R. C. Addis *et al.*, Optimization of direct fibroblast reprogramming to cardiomyocytes using calcium activity as a functional measure of success. *J. Mol. Cell. Cardiol.* **60**, 97–106 (2013).
37. P. J. Wrighton *et al.*, Signals from the surface modulate differentiation of human pluripotent stem cells through glycosaminoglycans and integrins. *Proc. Natl. Acad. Sci. U.S.A.* **111**, 18126–18131 (2014).
38. S. Zeng *et al.*, Telomerase-mediated telomere elongation from human blastocysts to embryonic stem cells. *J. Cell Sci.* **127**, 752–762 (2014).
39. T. Rivera, C. Haggblom, S. Cosconati, J. Karlseder, A balance between elongation and trimming regulates telomere stability in stem cells. *Nat. Struct. Mol. Biol.* **24**, 30–39 (2017).
40. K. Ufford *et al.*, Myofibrillar structural variability underlies contractile function in stem cell-derived cardiomyocytes. *Stem. Cell Rep.* **16**, 470–477 (2021).
41. S. Oikawa, S. Kawanishi, Site-specific DNA damage at GGG sequence by oxidative stress may accelerate telomere shortening. *FEBS Lett.* **453**, 365–368 (1999).
42. J. Tchou *et al.*, Substrate specificity of Fpg protein. Recognition and cleavage of oxidatively damaged DNA. *J. Biol. Chem.* **269**, 15318–15324 (1994).
43. J. Karlseder *et al.*, The telomeric protein TRF2 binds the ATM kinase and can inhibit the ATM-dependent DNA damage response. *PLoS Biol.* **2**, E240 (2004).
44. E. L. Denchi, T. de Lange, Protection of telomeres through independent control of ATM and ATR by TRF2 and POT1. *Nature* **448**, 1068–1071 (2007).
45. T. de Lange, Shelterin: The protein complex that shapes and safeguards human telomeres. *Genes Dev.* **19**, 2100–2110 (2005).

46. L.-J. Mah, A. El-Osta, T. C. Karagiannis, γH2AX: A sensitive molecular marker of DNA damage and repair. *Leukemia* **24**, 679–686 (2010).
47. A. Stolz, N. Ertych, H. Bastians, Tumor suppressor CHK2: Regulator of DNA damage response and mediator of chromosomal stability. *Clin. Cancer Res.* **17**, 401–405 (2011).
48. J. N. Weiss, A. Garfinkel, H. S. Karagueuzian, P.-S. Chen, Z. Qu, Early afterdepolarizations and cardiac arrhythmias. *Heart Rhythm.* **7**, 1891–1899 (2010).
49. B. van Steensel, A. Smogorzewska, T. de Lange, TRF2 protects human telomeres from end-to-end fusions. *Cell* **92**, 401–413 (1998).
50. D. Duan, N. Goemans, S. Takeda, E. Mercuri, A. Aartsma-Rus, Duchenne muscular dystrophy. *Nat. Rev. Dis. Primer* **7**, 13–19 (2021).
51. B. L. Prosser, C. W. Ward, W. J. Lederer, X-ROS signaling: Rapid mechano-chemo transduction in heart. *Science* **333**, 1440–1445 (2011).
52. G. Hewitt *et al.*, Telomeres are favoured targets of a persistent DNA damage response in ageing and stress-induced senescence. *Nat. Commun.* **3**, 708 (2012).
53. E. Sahin, R. A. DePinho, Linking functional decline of telomeres, mitochondria and stem cells during ageing. *Nature* **464**, 520–528 (2010).
54. I. Schmutz, L. Timashev, W. Xie, D. J. Patel, T. de Lange, TRF2 binds branched DNA to safeguard telomere integrity. *Nat. Struct. Mol. Biol.* **24**, 734–742 (2017).
55. F. Lottersberger, A. Bothmer, D. F. Robbiani, M. C. Nussenzweig, T. de Lange, Role of 53BP1 oligomerization in regulating double-strand break repair. *Proc. Natl. Acad. Sci. U.S.A.* **110**, 2146–2151 (2013).
56. P. Muñoz, R. Blanco, J. M. Flores, M. A. Blasco, XPF nuclease-dependent telomere loss and increased DNA damage in mice overexpressing TRF2 result in premature aging and cancer. *Nat. Genet.* **37**, 1063–1071 (2005).
57. B. Nera, H.-S. Huang, T. Lai, L. Xu, Elevated levels of TRF2 induce telomeric ultrafine anaphase bridges and rapid telomere deletions. *Nat. Commun.* **6**, 10132 (2015).
58. V. Codd *et al.*, Polygenic basis and biomedical consequences of telomere length variation. *Nat. Genet.* **53**, 1425–1433 (2021).
59. P. Martínez, M. A. Blasco, Heart-breaking telomeres. *Circ. Res.* **123**, 787–802 (2018).
60. C. Bär *et al.*, Telomerase gene therapy rescues telomere length, bone marrow aplasia, and survival in mice with aplastic anemia. *Blood* **127**, 1770–1779 (2016).
61. J. M. Povedano *et al.*, Therapeutic effects of telomerase in mice with pulmonary fibrosis induced by damage to the lungs and short telomeres. *Elife* **7**, e31299 (2018).
62. A. Derevyanko *et al.*, Gene therapy with the TRF1 telomere gene rescues decreased TRF1 levels with aging and prolongs mouse health span. *Aging Cell* **16**, 1353–1368 (2017).
63. J. Moslehi, R. A. DePinho, E. Sahin, Telomeres and mitochondria in the aging heart. *Circ. Res.* **110**, 1226–1237 (2012).